Clays and Clay Minerals, Vol. 60, No. 2, 99–107, 2012.

EFFECT OF Cd(II) ON THE RIPENING OF FERRIHYDRITE IN ALKALINE MEDIA

MARIANA ALVAREZ[1,*], MARÍA FERNANDA HORST[1], ELSA E. SILEO[2], AND ELSA H. RUEDA[1]

[1] INQUISUR, Departamento de Química, Universidad Nacional del Sur, Av. Alem 1253, B8000CPB, Bahía Blanca, Argentina
[2] INQUIMAE, Departamento de Química Inorgánica, Analítica y Química Física, Facultad de Ciencias Exactas y Naturales, Universidad de Buenos Aires, Pabellón II, Ciudad Universitaria, C1428EHA, Buenos Aires, Argentina

Abstract—To acquire a better understanding of the influence exerted by the presence of Cd^{2+} during the process of transforming ferrihydrite to goethite, the morphological and structural changes of several samples obtained by the addition of Cd^{2+} to a suspension of nascent goethite were explored, and their chemical reactivity in acid media assessed. The samples (series G_i) were obtained by adding, at different times during the synthesis process, Cd^{2+} ions to ferrihydrite ($Fe_5HO_8.4H_2O$) formed in alkaline media. The suspensions were aged for 5 days at 70ºC, and the amorphous materials were extracted using a HCl solution (series $G_{HCl\text{-}i}$). The X-ray diffraction (XRD) patterns showed that a goethite-like phase was formed, and chemical analyses indicated that the Cd content, x_{Cd}, increased with the earlier addition of the Cd^{2+} ions to the Fe oxyhydroxide suspension. Lattice parameters and cell volume, obtained by the Rietveld simulation of XRD data, indicated an enlargement of the cell parameters of goethite in line with the Cd-for-Fe substitution. In order to determine the influence of oxalate ions on the non-extracted solids, a second set of samples was also prepared that was kept in contact with an ammonium oxalate solution for 4 h (series $G_{ox\text{-}i}$). The dissolution behavior of two series of Cd goethites and of a third series, obtained from coprecipitation of Fe^{3+} and Cd^{2+} ions in alkaline media, was observed. Kinetics measurements in 4 M HCl showed that the initial dissolution rate of samples $G_{ox\text{-}i}$ decreased with aging time, while the opposite effect was observed for series $G_{HCl\text{-}i}$. Dissolution–time curves were well described by the Kabai equation, and activation energies were calculated using the Arrhenius equation. The results indicate that the presence of Cd during the crystallization process of goethite leads to the formation of a Cd goethite with modified morphology, structural parameters, and chemical reactivity.

Key Words—Acid Reactivity, Aging, Cadmium Incorporation, Goethite, HCl Extraction, Oxalate Extraction.

INTRODUCTION

Solid crystalline compounds such as Fe oxides can take up metals by isomorphic substitution. This substitution by other cations for Fe is often achieved through coprecipitation of the Fe oxide, and the replacing ions are subsequently strongly bound (Schultz *et al*., 1987; Ford *et al*., 1997). Isomorphic substitution may create structural defects in order to keep the overall distortion of the structure to a minimum. The size and valence of the guest ions are critical (Goldschmidt, 1937), and substitution by trivalent cations with a radius similar to that of Fe^{3+} is, therefore, most easily accommodated. This introduces only minor deformation of the mineral structure (Cornell and Schwertmann, 2003). Any replacement of Fe with foreign ions and the consequent occurrence of vacancies in the structure may alter the properties of the host mineral phase.

Several studies have analyzed the characteristics of synthetic substituted Fe oxides obtained by coprecipitation procedures (Cornell and Giovanoli, 1987; Martínez and McBride, 1998; Wells *et al*., 2001; Sileo *et al*., 2004; Wells *et al*., 2006; Alvarez *et al.* 2007, 2008; Kaur *et al.*, 2009); reports on the effects of adding cations to oxide particles as they form are scarce, though the effect of Mn^{2+} incorporation on the transformation of ferrihydrite to goethite has been studied (Alvarez *et al.*, 2005).

Amorphous Fe (oxyhydr)oxides can control the distribution and concentration of heavy metals in aqueous systems and have been used in environmental technologies to remove metals from wastewater and hazardous liquid waste (Benjamin *et al*., 1996), and in treatment of residues from air-pollution-remediation processes (Lundtorp *et al*., 2002). The removal of Cd from water *via* precipitation of hydrous oxides of Fe^{3+} and Mn^{4+} has been shown to be rapid and effective (Posselt and Weber, 1971).

Cadmium is not an abundant element but is distributed uniformly throughout most rocks on the Earth's crust (average content of 0.15–0.2 mg kg^{-1} Cd) (Sadiq, 1992). It is concentrated slightly in shales, especially in those rich in organic matter, in lacustrine and oceanic sediments, in manganese nodules, and in marine phosphorites. The chemistry of Cd in surface water and groundwater was reviewed by Hem (1972), who gave calculations of equilibrium solubilities with $Cd(OH)_2$ or $CdCO_3$, showing minimum solubility at pH 9.0–10.0. At pH < 6, Cd^{2+} is the soluble form of cadmium.

* E-mail address of corresponding author:
alvarezm@criba.edu.ar
DOI: 10.1346/CCMN.2012.0600201

The Cd^{2+} ion with a radius of 95 pm is the largest ion known to substitute for Fe^{3+} (64.5 pm) in the goethite structure. Recent studies of the structural modification of the goethite framework by Cd substitution (Sileo *et al*., 2003; Huynh *et al*., 2003) used conventional and synchrotron XRD, while the influence of Cd dopant on the properties of goethite and hematites in alkaline media were studied using Mössbauer spectroscopy (Krehula and Musić, 2007).

Another important aspect to consider is the effect of the substituent cation on the reactivity of Fe oxides synthesized in different media. Depending on the experimental conditions, one might expect a faster rate of dissolution of the substituted Fe oxides, but the opposite is often seen. This is interpreted to be the result of the formation of a protective surface layer (Cornell and Schwertmann, 2003).

Fe oxalate is formed as a product of decomposition of organic matter and is also generated by plant roots and microorganisms. For these reasons the oxalate anion ($C_2O_4^{2-}$) is found in a wide range of soil types, including cultivated soils, in concentrations ranging from a few to several hundred mM (Jones, 1998). Although most root exudates have a low affinity for Fe complexation, oxalate has a strong affinity for Fe in solution and at Fe-oxide surfaces (Filius *et al*., 1997; Jones and Brassington, 1998). Oxalate also precipitates with Cd, giving CdC_2O_4. In the dark, the anion can dissolve Fe oxides by a non-reductive ligand-controlled mechanism. In the presence of light, the anion dissolves the Fe oxides by a photochemical reductive mechanism producing aqueous Fe^{2+} and CO_2 (Sulzberger and Laubscher, 1995). Both mechanisms increase the bioavailability of Fe.

The aim of the present work was to acquire a better understanding of the effects of adding Cd^{2+}, at different times, on particles of ferryhidrite ($Fe_5HO_8.4H_2O$) that were transforming into goethite (α-FeOOH) in highly alkaline media, and to explore the behavior of the solids obtained in the presence of oxalate ions. The reactivity in acidic media of the several solids obtained was also assessed and compared with that of a series of Cd-goethites obtained in similar basic media by coprecipitation of both Cd and Fe cations (series S_i), already characterized from a structural point of view (Sileo *et al*., 2003).

MATERIALS AND METHODS

Preparation of the solids

A series of samples of goethite was synthesized following the procedure described by Sileo *et al*. (2003), by adding aqueous 1 M $Fe(NO_3)_3$ solution to a NaOH solution until the final $[OH^-]$ was 0.5 M. The suspensions formed were aged for 120 h at 70ºC in closed polyethylene flasks. Once the aging process had been initiated, 2.8 mL of a 1 M $Cd(NO_3)_2$ solution was added to each flask at 0, 2, 4, 8, and 12 h (the samples were named G_{120}, G_{118}, G_{116}, G_{112}, and G_{108}, respectively, where the subscript indicates the contact time in minutes bewteen Fe and Cd). The molar ratio for Cd in the preparation, x_{Cd}, in all samples, expressed as $100 \times n_{Cd}/(n_{Cd} + n_{Fe})$, was 5.5 mol.%, where n_{Cd} and n_{Fe} represent the moles of Cd and Fe in the initial solution. A blank of pure goethite was prepared in a similar way. Once a day, the flasks were shaken vigorously. The final products were centrifuged and washed three times with doubly distilled water. In order to remove any Cd or Fe cations not incorporated structurally in the goethite and to remove any ferrihydrite from the surface of the products, samples were soaked in 0.4 M HCl for 30 min, with a sample to acid ratio of 0.1 g to 100 cm^3 (Schwertmann and Cornell, 2000) (samples named $G_{HCl\text{-}i,}$). A second series was obtained by treating the 'as-synthesized' solids with 0.2 M oxalic acid/ammonium oxalate buffer (pH 3) at room temperature for 4 h with a solid:solution ratio = 1:100, according to specifications of Huynh *et al*. (2003) and Sileo *et al*. (2002) (samples named $G_{ox\text{-}i}$).

Chemical and morphological analyses

The Cd and Fe contents of the solids were determined by atomic absorption spectrometry using an ICP-OES Shimadzu Sequential 1000 Model III Spectrometer with pneumatic nebulization. The data were obtained in duplicate on 30 mg of each sample dissolved in 6 M HCl at 80ºC.

Particle morphologies were obtained by scanning electron microscopy (SEM) using a Field Emission Gun (FEG) Zeiss Supra 40 instrument operated at 5 keV. Samples were dispersed in double-distilled water with ultrasonic treatment and a drop of suspension was placed onto a metallic support.

XRD measurements

X-ray diffraction patterns were recorded with a Siemens D5000 diffractometer using CuKa radiation. Generator settings were 40 kV and 35 mA. A graphite diffracted-beam monochromator was used. Data were collected in the 15.800−140.000º2θ range, with a step size of 0.025º and a counting time of 15 s per step. The data were analyzed using the GSAS (Larson and Von Dreele, 1994) system and the EXPGUI interface (Toby, 2001).

Starting values of unit-cell parameters and atomic coordinates for goethite were taken from the literature (Szytula *et al*., 1968). Goethite is orthorhombic, space group *Pnma* (Z = 4); however, it is usually described using the *Pbnm* group. In order to facilitate comparisons with previous works, the refinement is presented here using the *Pbnm* group. Peak profiles were fitted using the Thompson-Cox-Hastings pseudo-Voigt function (Thompson *et al*., 1987) with the microstrain broadening description of Stephens (1999). Peak asymmetry was corrected using the Finger function (Finger *et al*., 1994).

https://doi.org/10.1346/CCMN.2012.0600201 Published online by Cambridge University Press

The measured background was fitted with a simple linear interpolation formula. Cell parameters and sample displacement, full width at half maximum, microstrain broadening parameters for the peak shape, scale factor, and positional and isotropic thermal parameters for all atoms were also refined. The preferred orientations were corrected in all samples by the March model (Dollase, 1986).

Thermogravimetric and Differential Thermal Analyses

Thermogravimetry-differential thermal analyses (TG-DTA) were obtained using a Rigaku Thermoflex TG 8110 Instrument, attached to a Therma Analysis Station TAS 100, in air atmosphere at a heating rate of 10ºC min^{-1}.

Infrared spectroscopy

Fourier-transform infrared (FTIR) spectra were recorded at room temperature using a Nicolet Nexus FTIR spectrometer (Norcross, Georgia, USA), at a resolution of 0.5 cm^{-1}. For each spectrum, 32 scans were accumulated. The specimens were pressed into small discs using a spectroscopically pure KBr matrix, in a ratio of 1:100.

Dissolution kinetics in HCl

Dissolution kinetics on series $G_{ox\text{-}i}$, $G_{HCl\text{-}i}$, and S_i (see below) was performed in air in a sealed cylindrical beaker provided with a thermostated water jacket and measured at temperatures from 40 to 60ºC. 50 mg of each sample was suspended in 50 cm^3 of 4 M HCl and the suspension stirred magnetically throughout the experiment. Subsamples (1 cm^3) of the reaction mixture were taken at intervals until total dissolution was achieved, and filtered using a syringe and a Nucleopore membrane (pore size = 0.22 mm). The amounts of Fe dissolved were determined by the o-phenanthroline method (Vogel, 1960). The amount of Fe per mole of oxide dissolved was plotted as a function of reaction time for each of the samples. The resulting dissolution curves were modeled, and the initial rate was calculated. All experiments were carried out in duplicate and the coefficient of variation was <0.08%.

Dissolution experiments were also carried out on a series of synthetic Cd goethites obtained by coprecipitation of both Cd and Fe cations (Series S_i), the structural characterization of which was established previously (Sileo *et al*., 2003).

RESULTS AND DISCUSSION

Chemical and physical analyses of the solids

Chemical analyses (Table 1) of the samples after ammonium oxalate and HCl extraction revealed that the Cd content in Series $G_{ox\text{-}i}$ remained essentially constant, indicating a leveling off in the total uptake of Cd ions. The x_{Cd} value in Series $G_{HCl\text{-}i}$ presented a marked decrease in Cd content with values that reached ~1/10 of the values found in series $G_{ox\text{-}i}$.

Laboratory XRD patterns of the samples extracted with ammonium oxalate (Series $G_{ox\text{-}i}$) showed that the main crystalline phase present was the goethite phase. In fact, the $G_{ox\text{-}120}$ diagram corresponds to a goethite-like structure. Samples G_{108} to G_{116} displayed additional peaks which correspond to increasing quantities of CdC_2O_4, indicating that the belated addition of Cd increased the CdC_2O_4 content (Figure 1).

All of the XRD patterns of the samples of Series $G_{HCl\text{-}i}$ presented a goethite-like structure. The patterns were modeled using the GSAS simulation program which utilizes the Rietveld method, a least-squares structural refinement technique in which the parameters of the structural model and of the instrument conditions are optimized simultaneously (Rietveld, 1969).

The refined cell parameters increased with increased contact time, resulting in a general increasing trend in the cell volumes from $G_{HCl\text{-}108}$ to $G_{HCl\text{-}120}$ (Table 2).

In the FTIR spectra of samples $G_{HCl\text{-}i}$, a broad band and a shoulder were observed at 3136–3167 cm^{-1} and 3450–3445 cm^{-1}, respectively. These signals were assigned to H–O–H and O–H stretching vibrations. A weak water-bending vibration at ~1790 cm^{-1} and the overtone of the OH-bending vibration (γ'(OH)) at 1633–1637 were detected. Intense hydroxyl deformation bands (δ(OH) and γ(OH) modes) were also found at 889 and 793–795 cm^{-1} (Ruan *et al*., 2001).

An intense band around 642 cm^{-1} due to lattice vibrations of FeO_6 groups (Ruan *et al*., 2001) was found for pure goethite. A further increase in Fe-Cd contact

Table 1. Cd contents, x_{Cd}, of the fresh samples (B) and after ammonium oxalate and HCl treatment ($G_{ox\text{-}i}$ and $G_{HCl\text{-}i}$ series, respectively).

Samples	x_{Cd} (mol.%)	Samples	x_{Cd} (mol.%)	Samples	x_{Cd} (mol.%)
B	0	B	0	B	0
G_{120}	0.1058	$G_{ox\text{-}120}$	0.067	$G_{HCl\text{-}120}$	0.0087
G_{118}	0.1047	$G_{ox\text{-}118}$	0.065	$G_{HCl\text{-}118}$	0.0062
G_{116}	0.1059	$G_{ox\text{-}116}$	0.064	$G_{HCl\text{-}116}$	0.0033
G_{112}	0.1018	$G_{ox\text{-}112}$	0.061	$G_{HCl\text{-}112}$	0.0017
G_{108}	0.1025	$G_{ox\text{-}108}$	0.069	$G_{HCl\text{-}108}$	0.0011

https://doi.org/10.1346/CCMN.2012.0600201 Published online by Cambridge University Press

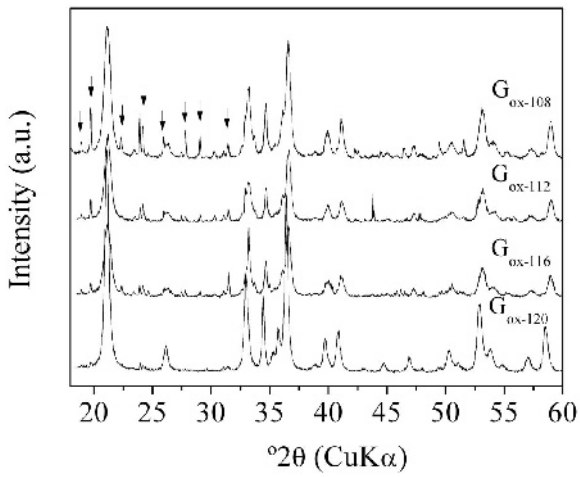

Figure 1. XRD patterns of samples in the $G_{ox\text{-}i}$ series. Arrows in sample $G_{ox\text{-}108}$ indicate the CdC_2O_4 mean peaks.

time (with a resultant increase in the amount of Cd^{2+} incorporated into the structural framework) gradually shifted the band to lower wavenumbers. In sample $G_{HCl\text{-}120}$ (with the greater Cd content) the band was found at 625 cm^{-1}.

The SEM images for selected samples of series $G_{HCl\text{-}i}$ (Figure 2) showed that the belated addition of Cd to the aging ferrihydrite decreased the length-width ratio of the acicular crystals formed. Previous data on coprecipitated Cd-Fe samples (Sileo *et al*., 2003) showed that an increase in x_{Cd} increased the length-width ratio. The changes observed indicate that Cd-for-Fe substitution in the goethite phase increased with the increase in Fe-Cd contact time. Elongation of α-FeOOH particles along the *c* axis was found for increasing Cd substitution, and Krehula and Musić (2007) assigned this effect to the formation of α-(Fe,Cd)OOH solid solutions upon Cd substitutions in octahedral sites.

For comparison, SEM images for samples $G_{ox\text{-}116}$ and $G_{HCl\text{-}116}$ (Figure 3) revealed that, although both samples show the same domain size, $G_{HCl\text{-}116}$ shows thinner and more defined needles.

Analyses by DTA of samples $G_{ox\text{-}108}$ and $G_{HCl\text{-}108}$ (Figure 4) revealed three well defined peaks (profile a): two endothermic, located at 87ºC and 264ºC, and one exothermic at 341ºC.

The broad endothermic peak centered at 87ºC was attributed to dehydration of Cd oxalate and the exothermic peak at 341ºC was attributed to the decomposition of CdC_2O_4 with the formation of CdO (Gabal, 2007). These peaks were absent from samples extracted with HCl acid, $G_{HCl\text{-}108}$ (profile b). The second endothermic peak, present in both samples, corresponded to the dehydroxylation temperature of goethite to form hematite.

Acid reactivity

Dissolution kinetics. All dissolution curves in both series $G_{ox\text{-}i}$ and $G_{HCl\text{-}i}$ show a sigmoidal shape (Figure 5).

Similar results were obtained by Cornell *et al.* (1974), Schwertmann (1984), and Schwertmann *et al.* (1985). Using transmission electron microscopy, Cornell *et al.* (1974) showed that the dissolution starts on the surface of the crystal and also at the interdomainal space. As a result, the crystals separate into domains and both the reacting surface and the reaction rate are increased.

Later, with reduction in reacting-surface space, the rate of dissolution decreased, a mechanism described by the modified Nernst equation (Kabai, 1973):

$$\ln\left[\ln\frac{C_0}{C_0 - C}\right] = \alpha \ln k + \alpha \ln t \qquad (1)$$

where C_0 is the initial amount of Fe, C is the amount of Fe dissolved at time t, a is a constant characteristic of the structure of the solid phase, and k is the dissolution rate constant.

The dissolution behavior in the oxalated-extracted samples (series $G_{ox\text{-}i}$) is not described fully by equation 1, and the plots conform approximately to two straight-line components.

The results agree with the findings of Schwertmann and Latham (1986) which indicated that dissolution

Table 2. Unit-cell parameters of samples of series $G_{HCl\text{-}i}$ obtained from XRD structural data.

Sample	*a* parameter (Å)	*b* parameter (Å)	*c* parameter (Å)	Volume (Å^3)	χ^2	R_{Bragg}*
$G_{HCl\text{-}120}$	4.6288(5)	10.0432(12)	3.0432(3)	141.473(27)	1.30	4.82
$G_{HCl\text{-}118}$	4.6204(6)	9.9755(8)	3.0306(3)	139.682(26)	1.64	4.4
$G_{HCl\text{-}116}$	4.6184(4)	9.9616(8)	3.0262(2)	139.225(20)	1.89	3.51
$G_{HCl\text{-}112}$	4.6161(4)	9.9604(7)	3.0253(2)	139.098(15)	1.71	8.90
$G_{HCl\text{-}108}$	4.6185(5)	9.9606(7)	3.0268(2)	139.212(22)	1.55	6.88

Values in parentheses are the estimated standard deviation.
* The R_{Bragg} factor is the Bragg-intensity R value and measures the agreement between the reflection intensities calculated from a crystallographic model and those measured experimentally. In the Rietveld method, R_{Bragg} is useful because it depends on the fit of the structural parameters and not on the profile parameters.

https://doi.org/10.1346/CCMN.2012.0600201 Published online by Cambridge University Press

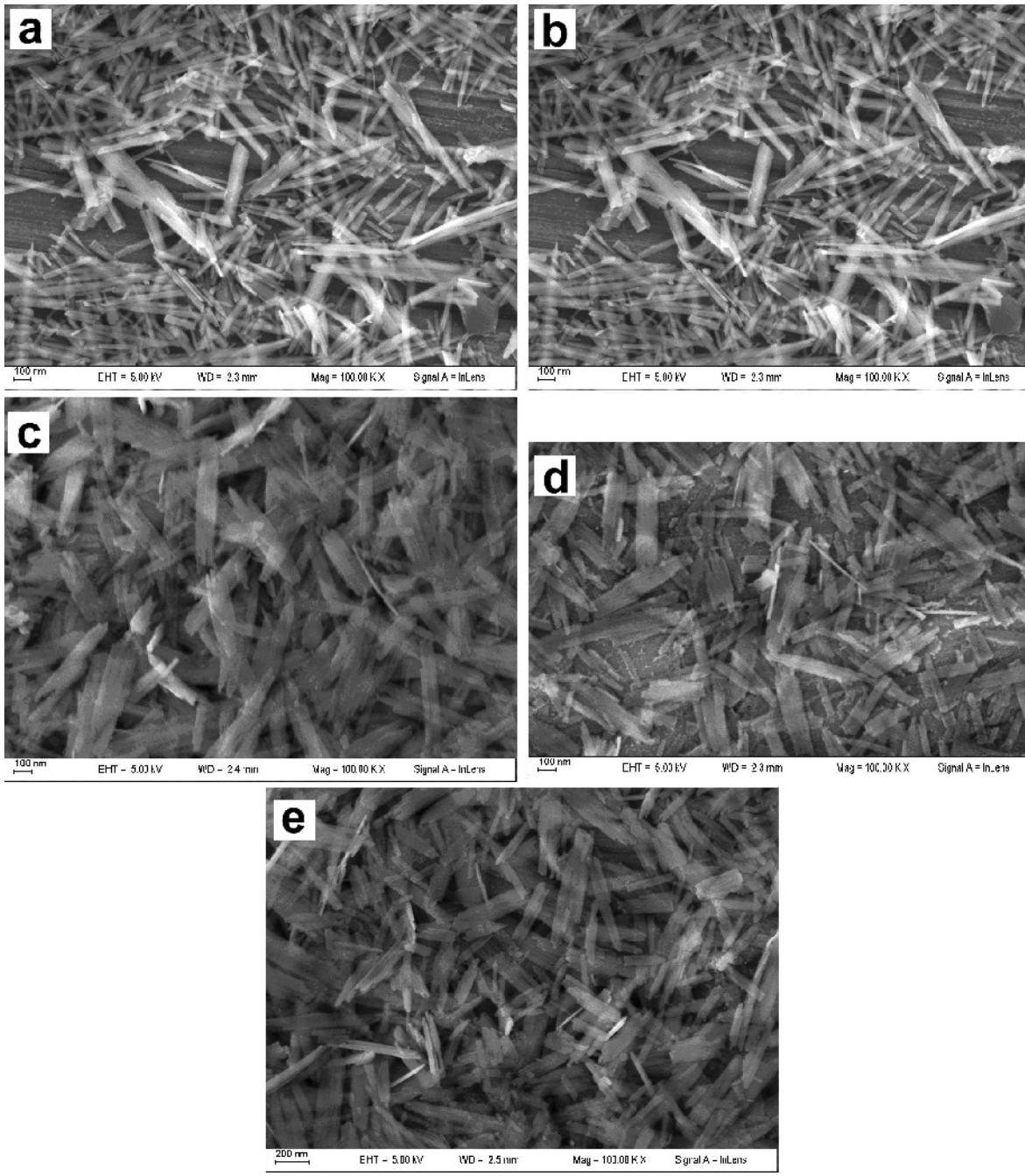

Figure 2. SEM images of samples (a) $G_{HCl\text{-}120}$, (b) $G_{HCl\text{-}118}$, (c) $G_{HCl\text{-}116}$, (d) $G_{HCl\text{-}112}$, and (e) $G_{HCl\text{-}108}$.

curves for natural samples containing a mixture of Fe oxides show two straight lines when fitted to equation 1. The behavior of $G_{ox\text{-}116}$, for example, is best described with two different lines. The first, with a smaller slope (0.921; $R^2 = 0.994$), follows equation 1 until 15% of the Fe has been dissolved, followed by a second line with a higher slope (1.640; $R^2 = 0.994$). On the other hand, the dissolution behavior of sample $G_{HCl\text{-}116}$, which contained no oxalate ions, is described well by a single straight line ($R^2 = 0.988$).

These observations support the suggestion of two phases of different reactivity in series $G_{ox\text{-}i}$, the first part of the kinetics being governed by the dissolution of a Cd-rich side compound and the second part being governed by the dissolution of pure Cd-substituted goethite.

https://doi.org/10.1346/CCMN.2012.0600201 Published online by Cambridge University Press

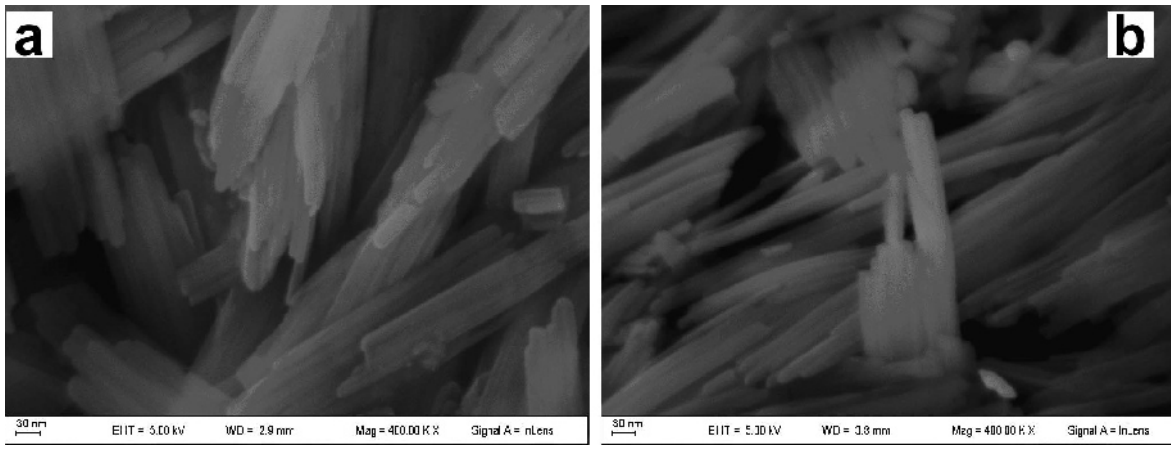

Figure 3. SEM images of samples (a) $G_{ox\text{-}116}$ and (b) $G_{HCl\text{-}116}$.

The release of Fe is practically identical for all samples in series $G_{ox\text{-}i}$ up to 200 min (Figure 5); differences in Fe release became significant after 60 min of dissolution time for series $G_{HCL\text{-}i}$. Such behavior could be attributed to the presence of the CdC_2O_4 phase in the G_i series.

Initial dissolution rate constants (k_i) (Table 3) show that the initial rate for the $G_{ox\text{-}i}$ series decreased with a small amount of Fe-Cd contact time and consequently with Cd content. Because the dissolution rate was calculated as a function of Fe released, the latter behavior could be attributed to a first attack produced over the Cd-rich phase which delayed the progress of the Fe dissolution.

Samples in series $G_{HCl\text{-}i}$ followed the opposite trend with k_i values increasing with the decrease of x_{Cd} in goethite. Kinetics measurements carried out on a series of Cd-Fe coprecipitated goethites (Series S_i, Table 3) obtained by Sileo *et al*. (2003) show similar kinetics features to this series of samples.

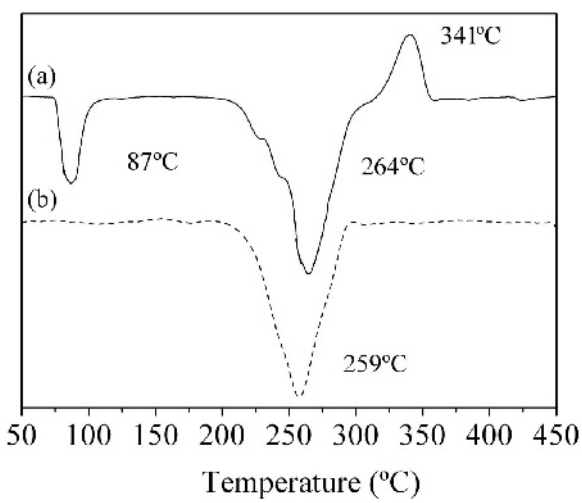

Figure 4. DTA curves from samples (a) $G_{ox\text{-}108}$ and (b) $G_{HCl\text{-}108}$.

Activation energy. Values of activation energy (E_a) for dissolution were obtained from the slope of plots of ln k_i *vs*. $1/T$ using the Arrhenius equation, with R^2 values

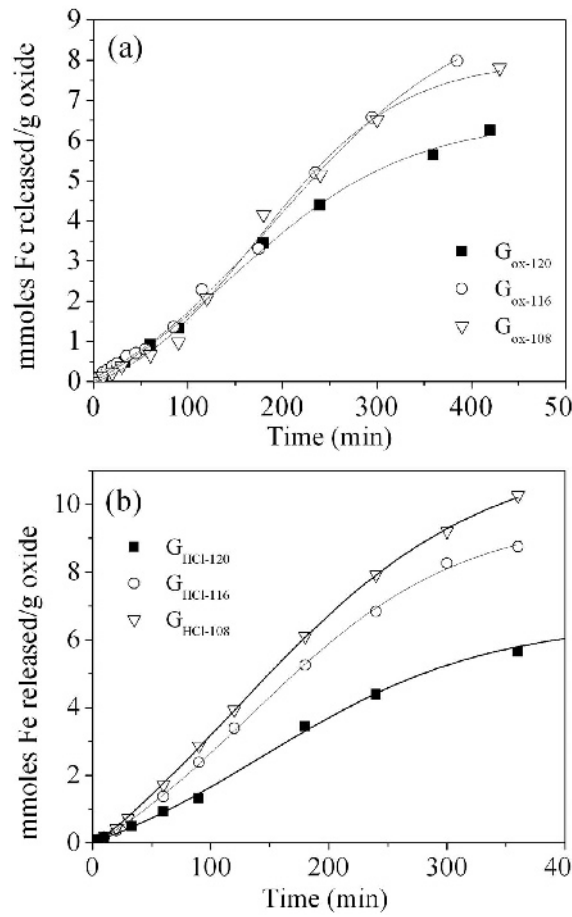

Figure 5. Representative dissolution curves for series (a) $G_{ox\text{-}i}$ and (b) $G_{HCl\text{-}i}$, expressed as mmoles of Fe dissolved g^{-1} of oxide in 4 M HCl at 40ºC *vs*. time.

https://doi.org/10.1346/CCMN.2012.0600201 Published online by Cambridge University Press

$\geqslant 0.98$ (Figure 6). The E_a values for samples $G_{ox\text{-}116}$ and $G_{HCl\text{-}116}$ were 140 and 127 kJ/mol, respectively. On the other hand, E_a values for samples $G_{ox\text{-}112}$ and $G_{HCl\text{-}112}$, with smaller Cd contents, were 147 and 135 kJ/mol, respectively. In each case, the clear decrease in E_a was attributed to the absence of CdC_2O_4 in the samples treated with HCl.

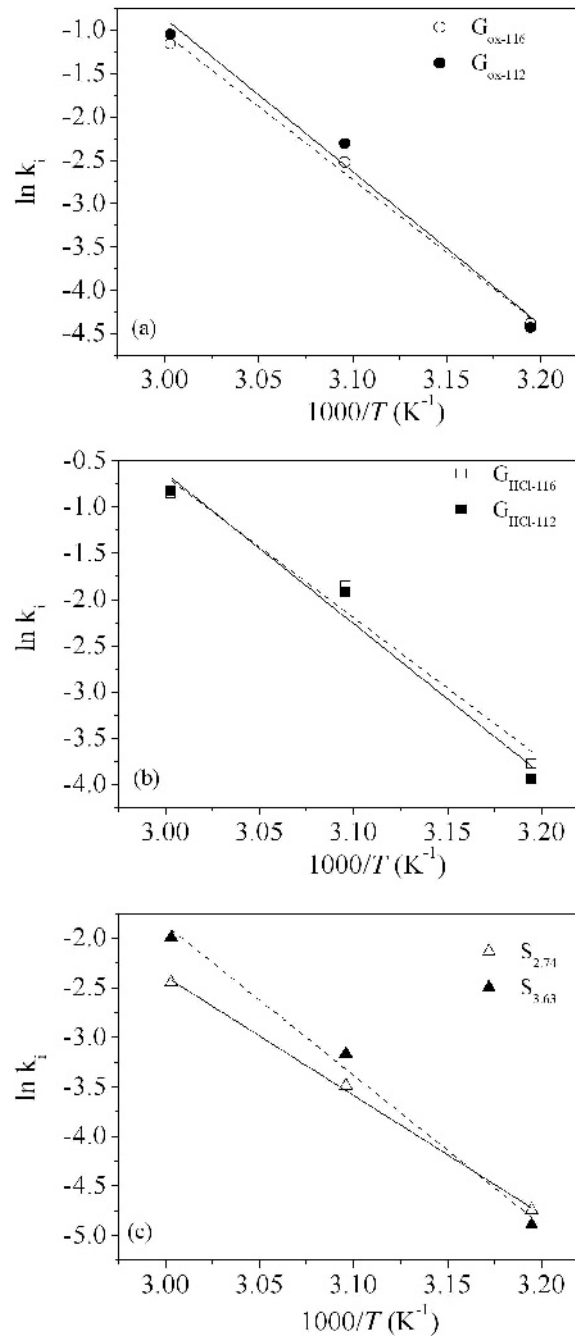

Figure 6. Arrhenius plots for rate constants, k_i, at different temperatures for selected samples from series (a) $G_{ox\text{-}i}$, (b) $G_{HCl\text{-}i}$, and (c) S_i.

Table 3. Initial rates of all series of Cd goethites ($\times 10^{-3}$).

$G_{ox\text{-}i}$ series	Initial rate, k_i ($\times 10^{-3}$) (mmoles Fe g_{ox}^{-1} min^{-1})	R^2	$G_{HCl\text{-}i}$ series	Initial rate, k_i ($\times 10^{-3}$) (mmoles Fe g_{ox}^{-1} min^{-1})	R^2	S_i series[a]	Initial rate, k_i ($\times 10^{-3}$) (mmoles Fe g_{ox}^{-1} min^{-1})	R^2
$G_{ox\text{-}120}$	14.4	0.989	$G_{HCl\text{-}120}$	14.4	0.991	$S_{5.50}$	5.4	0.999
$G_{ox\text{-}116}$	12.5	0.998	$G_{HCl\text{-}116}$	19.5	0.999	$S_{3.63}$	7.5	0.994
$G_{ox\text{-}112}$	11.9	0.993	$G_{HCl\text{-}112}$	22.9	0.998	$S_{2.74}$	8.7	0.996
$G_{ox\text{-}108}$	6.8	0.994	$G_{HCl\text{-}108}$	26.4	0.999	$S_{1.00}$	9.1	0.998

[a] Subscript indicates the Cd content expressed as mole%.

https://doi.org/10.1346/CCMN.2012.0600201 Published online by Cambridge University Press

The calculated E_a values for coprecipitated samples $S_{2.74}$ and $S_{3.63}$ were 99.7 and 126.0 kJ/mol, respectively.

Although the Fe−O and Cd−O bond lengths reported in the literature are 2.166 Å and 2.350 Å , respectively, E_a increased with increasing Cd content. Comparison of the E_a values in series $G_{HCl\text{-}i}$ and S_i showed that the dissolution rates were affected not only by the Cd content but also by the way in which the Cd was incorporated.

CONCLUSIONS

Incorporation of Cd at different times during the crystallization process of goethite determined the Cd content in the oxide structure. In spite of the increase in the unit-cell volume, goethite was stabilized against dissolution by the presence of Cd in its framework. Increase in Cd-Fe contact time produced larger needles. The initial dissolution rate increased with decrease in Cd incorporation, and samples with greater Cd content were less soluble in HCl. The same results were obtained in coprecipitate and HCl-extracted samples. When the solids were kept in contact with an ammonium oxalate solution, a layer of Cd-oxalate was formed on the surface of the crystallites stabilizing the solid against dissolution. The present results agree with the E_a values found for the different series: $G_{ox\text{-}i}$, $G_{HCl\text{-}i}$, and S_i.

The results above seem to suggest that inorganic pollutants such as Cd could be retained and immobilized by a naturally aged Fe (oxyhydr)oxide sludge. The results also indicate that oxalate ions formed a layer on the Cd-containing solids that stabilized the solid against dissolution. Modifications of the goethite design (either by isostructural modification or by formation of protective layers over the oxide) may offer promise for specific uses such as water purification.

ACKNOWLEDGMENTS

This work was supported partially by Grants PICT 2008, Nº 0780 and SGCyT 24/Q030 from the Universidad Nacional del Sur. The authors thank the reviewers for their insightful comments.

REFERENCES

Alvarez, M., Sileo, E.E., and Rueda, E.H. (2005) Effect of Mn(II) incorporation on the transformation of ferrihydrite to goethite. *Chemical Geology*, **216**, 89−97.

Alvarez, M., Rueda, E.H., and Sileo, E.E. (2007) Simultaneous incorporation of Mn and Al in the goethite structure. *Geochimica et Cosmochimica Acta*, **71**, 1009−1020.

Alvarez, M., Sileo, E.E., and Rueda, E.H. (2008) Structure and reactivity of synthetic Co-substituted goethites. *American Mineralogist*, **93**, 584−590.

Benjamin, M.M., Sletten, R.S., Bailey, R.P., and Bennett, T. (1996) Sorption and filtration of metals using iron-oxide coated sand. *Water Research*, **30**, 2609−2620.

Cornell, R.M. and Giovanoli, R. (1987) Effect of manganese on the transformation of ferrihydrite into goethite and jacobsite in alkaline media. *Clays and Clay Minerals*, **35**, 11−20.

Cornell, R.M., Posner, A.M., and Quirk, J.P. (1974) Crystal morphology and the dissolution of goethite. *Journal of Inorganic and Nuclear Chemistry*, **36**, 1937−1946.

Cornell, R.M. and Schwertmann, U. (2003) *The Iron Oxides*, 2nd edition. Wiley-VCH, New York, 664 pp.

Dollase, W.A. (1986) Corrections of intensities for preferred orientations in powder diffractometry: Applications of the March model. *Journal of Applied Crystallography*, **19**, 267−272.

Filius, J.D., Hiemstra, T., and van Riemsdijk, W.H. (1997) Adsorption of small weak organic acids on goethite: Modeling of mechanisms. *Journal of Colloid and Interface Science*, **195**, 368−380.

Finger, L.W., Cox, D.E., and Jephcoat, A.P. (1994) A correction for powder diffraction peak asymmetry due to axial divergence. *Journal of Applied Crystallography*, **27**, 892−900.

Ford, R.G., Bertsch, P.M., and Farley, K.J. (1997) Changes in transition and heavy metal partitioning during hydrous iron oxide aging. *Environmental Science & Technology*, **31**, 2028−2033.

Gabal, M.A. (2007) Non-isothermal kinetics and characterization studies for the decomposition course of CuC_2O_4−CdC_2O_4 mixture in air. *Journal of Physics and Chemistry of Solids*, **68**, 1610−1616.

Goldschmidt, V.M. (1937) The principles of distribution of chemical elements in minerals and rocks. *Journal of Chemical Society*, 655−673.

Hem, J.D. (1972) Chemistry and occurrence of cadmium and zinc in surface and ground water. *Water Resources Research*, **8**, 661−679.

Huynh, T., Tong, A.R., Singh, B., and Kennedy, B.J. (2003) Cd-substituted goethites – A structural investigation by synchrotron X-ray diffraction. *Clays and Clay Minerals*, **51**, 397−402.

Jones, D.L. (1998) Organic acids in the rhizosphere – a critical review. *Plant Soil*, **205**, 25−44.

Jones, D.L. and Brassington, D.S. (1998) Sorption of organic acids in acid soils and its implications in the rhizosphere. *European Journal of Soil Science*, **49**, 447−455.

Kabai, J. (1973) Determination of specific activation energies of metal oxides and metal oxide hydrates by measurement of the rate of dissolution. *Acta Chimica Academiae Scientarium Hungaricae*, **78**, 57−73.

Kaur, N., Singh, B., and Kennedy, B. (2009) Copper substitution alone and in the presence of chromium, zinc, cadmium and lead in goethite (α-FeOOH). *Clay Minerals*, **44**, 293−310.

Kaur, N., Gräfe, M., Singh, B., and Kennedy, B. (2009) Simultaneous incorporation of Cr, Zn, Cd, and Pb in the goethite structure. *Clays and Clay Minerals*, **57**, 234−250.

Krehula, S. and Musić, S. (2007) The influence of Cd-dopant on the properties of α-FeOOH and α-Fe_2O_3 particles precipitated in highly alkaline media. *Journal of Alloys and Compounds*, **431**, 56−64.

Larson, A.C. and Von Dreele, R.B. (1994) *General Structure Analysis System* (GSAS), Los Alamos National Laboratory report LAUR 86-748.

Lundtorp, K., Jensen, D.L., Sørensen, M.A., Christensen, T.H., and Mogensen, E.P.B. (2002) Treatment of waste incinerator air-pollution-control residues with $FeSO_4$: Concept and product characterisation. *Waste Management & Research*, **20**, 1, 69−79.

Martínez, C.E. and McBride, M. (1998) Coprecipitates of Cd, Cu, Pb and Zn in iron oxides: solid phase transformation and metal solubility after aging and thermal treatment. *Clays and Clay Minerals*, **46**, 537−545.

Posselt, H.S. and Weber Jr., W.J. (1971) Environmental

chemistry of cadmium in aqueous systems. Tech Rept. T-71-1, University of Michigan, Ann Arbor, Michigan, USA.

Rietveld, H.M. (1969) A profile refinement method for nuclear and magnetic structures. *Journal of Applied Crystallography B*, **25**, 925–46.

Ruan, H.D., Frost, R.L., and Kloprogge, J.T. (2001) The behavior of hydroxyl units of synthetic goethite and its dehydroxylated product hematite. *Spectrochimica Acta Part A*, **57**, 2575–2586.

Sadiq, M. (1992) *Toxic Metal Chemistry in Marine Environments*. Marcel Dekker Inc. New York, 390 pp.

Schultz, M.F., Benjamin, M.M., and Ferguson, J.F. (1987) Adsorption and desorption of metals on ferrihydrite: Reversibility of the reaction and sorption properties of the regenerated solid. *Environmental Science & Technology*, **21**, 863–869.

Schwertmann, U. (1984) The influence of aluminium on iron oxides: IX. Dissolution of Al-goethites in 6 M HCl. *Clay Minerals*, **19**, 9–19.

Schwertmann, U., Cambier, P., and Murad, E. (1985) Properties of goethites of varying crystallinity. *Clays and Clay Minerals*, **33**, 369–378.

Schwertmann, U. and Cornell, R.M. (2000) *Iron Oxides in the Laboratory. Preparation and Characterization*, 2nd edition. Wiley, VCH, New York, 188 pp.

Schwertmann, U. and Latham, M. (1986) Properties of iron oxides in some New Caledonian oxisols. *Geoderma*, **39**, 105–123.

Sileo, E.E., Solís, P.S., and Paiva-Santos, C.O. (2003) Structural study of a series of synthetic goethites obtained in aqueous solutions containing cadmium (II) ions. *Powder Diffraction*, **18**, 49–55.

Sileo, E.E., Ramos, A.Y., Magaz, G.E., and Blesa, M.A. (2004) Long-range vs. short-range ordering in synthetic Cr-substituted goethites. *Geochimica et Cosmochimica Acta*, **68**, 3053–3063.

Stephens, P.W. (1999) Phenomenological model of anisotropic bradening in powder diffraction. *Journal of Applied Crystallography*, **32**, 281–289.

Sulzberger, B. and Laubscher, H. (1995) Reactivity of various types of iron (III) (hydr)oxides towards light-induced dissolution. *Marine Chemistry*, **50**, 103–115.

Szytula, A., Burewicz, A., Dimitrijewic, Z., Krasnicki, S., Rzany, H., Todorovic, J., Wanic, A., and Wolski, W. (1968) Neutron diffraction studies of α-FeOOH. *Physica Status Solidi*, **26**, 429–434.

Thompson, P., Cox, D.E., and Hastings, J.B. (1987) Rietveld refinement of Debye-Scherrer synchrotron X-ray data from Al_2O_3. *Journal of Applied Crystallography*, **20**, 79–83.

Toby, B.H. (2001) EXPGUI, a graphical user interface for GSAS. *Journal of Applied Crystallography*, **34**, 210–213.

Vogel, A.I. (1960) *Química Analítica Cuantitativa.* Volumen II. Química Analítica Aplicada, Análisis Instrumental y Análisis de Gases. Editorial Kapelusz, Buenos Aires, Argentina, 1173 pp.

Wells, M.A., Gilkes, R.J., and Fitzpatrick, R.W. (2001) Properties and acid dissolution of metal-substituted hematites. *Clays and Clay Minerals*, **49**, 60–72.

Wells, M.A., Fitzpatrick, R.W., and Gilkes, R.J. (2006) Thermal and mineral properties of Al-, Cr-, Mn-, Ni- and Ti-substituted goethite. *Clays and Clay Minerals*, **54**, 176–194.

(*Received 12 March 2010; revised 11 October 2011; Ms. 418; A.E. J.D. Fabris*)